Nano Research

Open Access

Research Article

Synthesis of methanol via CO_2 hydrogenation catalyzed by $La_2O_2CO_3$/Cu catalysts

Jun He[1,2], Chenglong Yu[1,3], Zhijuan Zhao[4], Bo Guan[4], Bin Zhang[1], Yanru Zhang[1,3], Longbo Zhang[1,3], Yanyan Wang[1,3], Ying Wang[1], Yahui Wu[1], Jia Guo[1,3], Yang Li[1,3], Tianbin Wu[1], Qingli Qian[1,3] ✉, Hongxing Wang[2] ✉, and Buxing Han[1,3,5] ✉

[1] *Beijing National Laboratory for Molecular Sciences, Key Laboratory of Colloid and Interface and Thermodynamics, Center for Carbon Neutral Chemistry, Institute of Chemistry, Chinese Academy of Sciences, Beijing 100190, China*
[2] *College of Chemical Engineering and Materials Science, Tianjin University of Science and Technology, Tianjin 300457, China*
[3] *School of Chemical Sciences, University of Chinese Academy of Sciences, Beijing 100049, China*
[4] *Center for Physicochemical Analysis Measurements, Institute of Chemistry, Chinese Academy of Sciences, Beijing 100190, China*
[5] *Shanghai Key Laboratory of Green Chemistry and Chemical Processes, State Key Laboratory of Petroleum Molecular and Process Engineering, School of Chemistry and Molecular Engineering, East China Normal University, Shanghai 200062, China*

Cite this article: *Nano Research*, **2025**, *18*, 94907130. https://doi.org/10.26599/NR.2025.94907130

ABSTRACT: The development of efficient Cu-based heterogeneous catalysts for CO_2 hydrogenation to methanol has been an appealing subject. Inspired by the concept of inverse catalysts, a series of $La_2O_2CO_3$/Cu nanorod composites with varying Cu contents (denoted as LOC/Cu-*x*, where *x* stands for the mass ratio of La and Cu in the catalysts) were prepared by combining coprecipitation and calcination processes. Remarkable composition-dependence of catalytic activity and selectivity were observed when different LOC/Cu-*x* (*x* = 0.1, 0.2, 0.5, 1, 3 and 5) were used to catalyze the CO_2 hydrogenation. The predominant product shifted from methane to methanol with the increasing Cu content. The highest reaction rate (13.3 mmol·g_{Cu}^{-1}·h^{-1}) and methanol selectivity (85.5%) were achieved when LOC/Cu-1 was tested at 200 °C. The LOC was not active for the reaction, while the Cu itself displayed poor catalytic performance. The Cu–LOC interactions significantly affected the nature of the catalysts, including mutual electron transfer, crystal structure, morphology, porosity, surface Cu valence and capability of adsorbing the reactant gases, etc., which account for the outstanding behavior of the LOC/Cu-1 catalyst. This work provides a new strategy for the design and optimization of Cu-based catalysts.

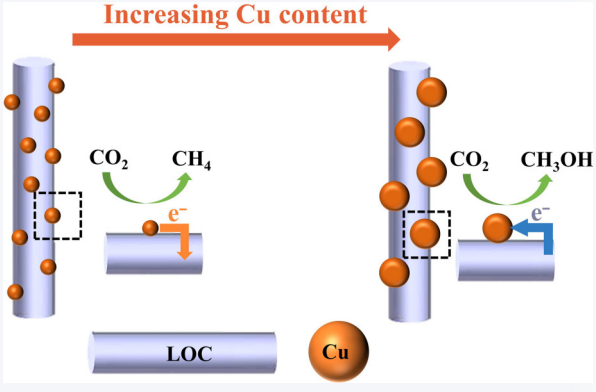

KEYWORDS: CO_2 hydrogenation, methanol, heterogeneous catalysts, Cu–$La_2O_2CO_3$ (LOC) interaction

1 Introduction

The escalating amount of CO_2 in the atmosphere caused by human activities, has led to climate change and environmental problems, such as rising sea levels, melting glaciers and extreme weather events. One of the most promising methods to mitigate the negative impacts of CO_2 emissions is to transform the CO_2 resource into value-added products, such as hydrocarbons, alcohols, and carboxylic acids [1–12]. Among all the various options for CO_2 conversion, the hydrogenation of CO_2 to methanol has garnered significant attention due to its ease transportation and efficient utilization as a fuel [13]. Therefore, the development of efficient catalysts for methanol synthesis has aroused considerable interest worldwide.

Over the decades, the Cu-based catalysts have been extensively studied due to their abundant reserves and high methanol selectivity. Unfortunately, bare Cu could hardly activate CO_2, as confirmed by both experimental and theoretical results, and the competitive reverse water gas shift (RWGS) reaction tended to suppress the methanol selectivity [14]. Until now, a growing number of researchers have perceived that constructing of Cu-oxides interface was a simple and efficacious way to inhibit the

Received: September 15, 2024; **Revised:** November 8, 2024
Accepted: November 13, 2024

✉Address correspondence to Qingli Qian, qianql@iccas.ac.cn; Hongxing Wang, wanghx@tust.edu.cn; Buxing Han, hanbx@iccas.ac.cn

RWGS reaction and enhance CO_2 affinity. Various oxides and mixed oxides such as ZnO, ZrO_2 and ZnO/Ga_2O_3 have been demonstrated as good supports [15–17]. For example, Liao et al. maximized the interface area of Cu-ZnO via morphological regulation, and observed that the polar facets of ZnO benefited methanol synthesis [18]. In addition to morphological control, other strategies such as doping metal compounds [19], improving the dispersion of Cu [20] and constructing defective oxides [21] had also been reported to be helpful in maximizing the interface area and optimizing the structure of the active interface, which could enhance methanol production. Recently, Ma's group developed an inverse ZrO_2/Cu catalyst with 90% Cu, which owned the same interface structure as traditional Cu/ZrO_2 catalyst with 10% Cu, while it exhibited approximately 3 times higher activity toward methanol yield than traditional catalyst [22]. With the development of inverse catalyst, scientists have realized that the neglected loading content of Cu might also play a critical role in the catalytic performance. However, very limited work focused on it toward slurry CO_2 hydrogenation.

$La_2O_2CO_3$ (LOC), a recently concerned basic oxide, has attracted considerable interest and is considered a promising candidate as a support or promoter material due to its medium surface basicity, excellent thermal stability and good coke resistance [23, 24]. It has been extensively investigated in dry methane reforming (DRM), RWGS and CO_2 methanation reactions, showing expectational performance [25–27]. Previous studies suggested that increased surface basicity was conductive to chemisorb CO_2 while strong basic sites would hinder the release of certain intermediates during the catalytic process. This implied that LOC, with moderate basicity, could balance the CO_2 adsorption and the transformation of intermediates [28, 29]. In addition, besides enhancing the dispersion and stability of metal particles, LOC also exhibited a stronger electrical interaction with the active component than other typical oxides, playing a pivotal role in selectivity regulation [25]. Therefore, LOC showed promising potential for fabricating supported Cu-based catalyst toward methanol synthesis via CO_2 hydrogenation.

Based on the above discussion, herein, a series of $La_2O_2CO_3$/Cu nanorod composites with varying Cu contents (denoted as LOC/Cu-*x*, where *x* stands for the mass ratio of La and Cu in the catalysts) were prepared by the coprecipitation-calcination method. The effects of Cu content on the microstructure and electronic state of LOC/Cu-*x* were studied using several characterization methods. Subsequently, the catalytic performance of the LOC/Cu-*x* on CO_2 hydrogenation was evaluated, and the optimal Cu content was determined. Detailed study demonstrated that the strong Cu–LOC interaction played a crucial role in enhancing the catalytic performance. This work highlights a new approach to optimize Cu-based catalysts for methanol production.

2 Experimental

2.1 Catalyst preparation

A series of LOC/Cu-*x* catalysts with different Cu contents were prepared by a facile method, involving a two-step precipitation in one-pot followed by an annealing process. $Cu(NO_3)_2{\cdot}xH_2O$ and $La(NO_3)_3{\cdot}xH_2O$ were selected as starting materials, with $CO(NH_2)_2$ as the additive and NaOH as the precipitation agent. The procedure for the two-step precipitation was as follows: a certain amount of $Cu(NO_3)_2{\cdot}xH_2O$, $La(NO_3)_3{\cdot}xH_2O$ and $CO(NH_2)_2$ (5 g) were dissolved in deionized water to form a clear solution (the amounts of the starting materials for different catalyst compositions were given in Table S1 in the Electronic Supplementary Material (ESM)). The mixture was continuously stirred at 80 °C for 3 h, resulting in a blue suspension (the first-step precipitation). Subsequently, certain amount of 2 M NaOH solution was gradually added dropwise to adjust the pH value to 7–8, leading to the formation of a coffee brown precursor precipitate (the second-step precipitation). The precipitate was separated through centrifugation, then washed with water and dried at 60 °C for 12 h. Then the dried samples were calcined at 500 °C for 4 h. Finally, the catalysts were reduced at 300 °C under H_2/Ar (10 vol.%) atmosphere for 2 h to activate the surface oxygen defects. The collected samples were denoted as LOC/Cu-*x* (*x* = 0.1, 0.2, 0.5, 1, 3 and 5), where x represented the mass ratio of La and Cu in the catalysts. Pure LOC was prepared using the same procedure except the addition of Cu. The information of the chemicals used for catalyst preparation was supplied in the ESM.

2.2 *In situ* and semi *in situ* characterization

The semi *in situ* X-ray photoelectron spectroscopy (XPS) measurement was aided by a special vacuum seal sample unit to transfer the sample prepared in the glove box. To study the CO_2 adsorption, LOC/Cu-1 was pretreated with 3 MPa of H_2 at 200 °C for 2 h. The reactor was cooled, and the H_2 was released and replaced with 1 MPa of CO_2 three times. Then the reactor was charged with 1 MPa of CO_2 and kept at the specified temperature for 1 h. Finally, the reactor was cooled to room temperature, and the gases were released. The sample was prepared in a glove box, and transferred to the sample chamber of an XPS spectrometer using the sample unit. To reduce the loss of adsorbates during the XPS analysis, the sample chamber was kept at ultra-low temperature using liquid nitrogen.

The *in situ* Fourier transform infrared (FTIR) spectroscopy spectra were recorded with a FOLI10-R-T infrared spectrometer equipped with a DLaTGS detector supplied by INSA Co. Ltd. The measurements were conducted in transmission mode at a resolution of 4 cm^{-1}, with a scanning speed of one spectrum per minute. Preceding CO_2 adsorption, the catalyst underwent treatment in 10% H_2/Ar at 200 °C for 2 h. After the mixture was cooled to 150 °C, the background spectrum was recorded. Subsequently, pure CO_2 was introduced into the *in situ* reaction cell, and spectra were continuously collected until no further changes were observed. Other methods of catalyst characterization were stated in the ESM.

2.3 Catalytic reaction

The CO_2 hydrogenation was conducted in a 16 mL stainless steel batch reactor that had a Teflon lining. In a typical experiment, 20 mg of catalyst and 2 mL of solvent were added to the reactor. Then the reactor was purged three times with 1 MPa CO_2 at room temperature to remove the remaining air. Subsequently, CO_2 and H_2 under specific pressure were introduced into the reactor at room temperature, then the reaction was conducted at a fixed temperature. After completion, the reactor was thoroughly cooled in an ice-water bath, and the gas was slowly released and collected in a gasbag. The gaseous samples were analyzed using a gas chromatograph (GC, Agilent 4890D) equipped with a thermal conductivity detector (TCD) and a packed column (Carbon

molecular sieve TDX-01, 3 mm in diameter and 1 m in length), using argon as the carrier gas. The liquid products were analyzed using an HP 7890B gas chromatograph with a flame ionization detector, and toluene was used as an internal standard. The identification of liquid products was performed using GC-mass spectrometry (GC-MS, Agilent-7890B-5977A) by comparing the retention times with standards in the GC traces. The selectivity of the products was calculated based on the GC data.

2.4 The recycling test

The solid catalyst was separated and washed with water and acetone for several times, followed by drying under vacuum at 60 °C for 12 h. Afterward, the catalyst was directly employed for the subsequent reaction.

3 Results and discussion

3.1 Catalyst characterizations

A series of LOC/Cu-*x* catalysts with different Cu contents were synthesized via combining coprecipitation and calcination method, the actual concentrations of Cu and La were determined using inductively coupled plasma-optical emission spectroscopy (ICP-OES), and the actual mass ratios of La to Cu were close to the designed values (Table S2 in the ESM). The sintering temperature of 500 °C was adopted based on the thermogravimetric analysis-differential thermal analysis (TGA-DTA) results, and LOC and CuO were formed after calcination (Fig. S1 in the ESM). The following reduction temperature of 300 °C was determined based on the H_2-temperature programmed reduction (TPR) results to ensure transformation from CuO to Cu (Fig. S2 in the ESM). A slight variation in the crystal structure (monoclinic and hexagonal phase) for LOC was also observed during the reduction of the calcined LOC/Cu-*x* (Fig. 1(a) and Fig. S1(a) in the ESM) [30, 31]. For the calcined catalysts, the diffraction peaks at 12.7°, 23.1°, 29.6° and 31° were attributed to monoclinic $La_2O_2CO_3$ (JCPDS 48-1113), while those at approximately 25.5°, 30.3°, 44.1° and 54.4° were attributed to hexagonal $La_2O_2CO_3$ (JCPDS 37-0804), indicating that the synthesized hybrids comprised both of the above phases [32]. With the increase of the La/Cu mass ratio, the relative content of these two types of $La_2O_2CO_3$ crystal structures also changed. We also observed the peak of metallic Cu in the reduced catalyst (Fig. 1(a)). FTIR spectroscopy was also performed to investigate the surface functional group of LOC/Cu-*x* (Fig. 1(b)) [33]. The band around 2338 cm^{-1} could be ascribed to the oscillations of atmospheric CO_2 [34]. The band observed at 3453 and 1642 cm^{-1} corresponding to the O–H vibration of water absorbed onto the catalyst surface [35]. The characteristic bands appeared at 1352 and 1467 cm^{-1} were assigned to the absorption peaks of CO_3^{2-}, and their intensity increased with the increasing *x* value [36]. The band corresponding to the stretching vibration of CH_2 occurred at 852 cm^{-1} and the bending vibration of La–O appeared at 481 cm^{-1} [37, 38].

XPS measurement was employed to investigate the valence state and surface composition of the catalysts [39]. For Cu 2p orbits, signals appeared only at ~ 932 and ~ 952 eV and no satellite peak was observed at higher Cu content, suggesting that surface Cu^{2+} species were mostly reduced to Cu^0 after the reduction process (Fig. 1(c)) [40]. Cu LMM further proved that Cu^0 was the main state, especially at higher Cu content (Fig. 1(d)). It was noteworthy that the Cu 2p spectra shift towards lower binding energy at high Cu content, indicating the electrons transfer from LOC to Cu and formation of more negative Cu surface. On the contrary, at low Cu content, the electrons transferred from Cu to LOC, generating more Cu^+/Cu^{2+} on catalyst surface. These phenomena suggested the strong interaction between Cu and LOC (the binding energy of Cu $2p_{3/2}$ was ~ 933 eV for bulk Cu). The electrons transfer usually exerted a marked impact on the catalytic performance of a catalyst. La 3d orbitals featured two doublets, the characteristic peaks of La $3d_{5/2}$ and La $3d_{3/2}$ were located at about 834.7 and 851.4 eV, respectively (Fig. 1(e)). It was obvious that the La $3d_{3/2}$ and $3d_{5/2}$ states had an energy difference of approximately 17 eV, which was a value consistent with the expected characteristics of La^{3+} [41, 42]. The O 1s spectra were deconvoluted into three distinct peaks: lattice oxygen ($O_{lattice}$), surface oxygen defects (O_{defect}) and hydroxyl groups (Ads.*OH) (Fig. 1(f)) [43]. At higher Cu content the $O_{lattice}$ gradually became significant, which might be from the Cu oxide nanophase. At lower Cu content the $O_{lattice}$ located at about 1 eV below gradually became obvious, which might be from the La oxides. The $O_{lattice}$ of LOC/Cu-1 was the weakest among the LOC/Cu-*x* catalysts, indicating the best fusion of the Cu and La species. The C 1s spectra also confirmed the existence of CO_3^{2-} species, which might be ascribed to the LOC (Fig. S3 in the ESM).

To further identify the surface morphology and metal dispersion on the catalysts, scanning electron microscopy (SEM) and transmission electron microscopy (TEM) images were taken for the LOC/Cu-*x* catalysts. As shown in the SEM images, the LOC exhibited a rod-like morphology with lengths of about 100–200 nm and it could be clearly seen at the lower Cu content (Figs. 2(a)–2(c)). However, severe agglomeration occurred at higher Cu content (Figs. 2(d)–2(f)). The microstructure of LOC/Cu-1 was further examined by TEM and high-resolution TEM (HRTEM) characterizations. The LOC exhibited a rod shape and Cu particles were dispersed on the LOC surface (Fig. 2(g)). The lattice spacing of 0.35 and 0.31 nm corresponded to the (100) facet of metallic Cu and (130) facet of LOC (Fig. 2(h)), which was consistent with X-ray diffraction (XRD) results. The energy dispersive spectroscopy (EDS) results showed that the Cu and La dispersed very well on the catalyst (Fig. 2(i)). In addition, the concentration of the Cu on the LOC/Cu-*x* gradually increased with the decreased x value, which agreed with the ICP-OES results (Fig. S4 in the ESM).

The impact of the Cu content on the physical structure of the LOC/Cu-*x* catalysts could also be reflected by the N_2 adsorption–desorption characterization. To a certain extent, all catalysts exhibited type IV isotherm loops (Fig. 3(a)), the surface areas (S_{BET}, BET: Brunauer–Emmett–Teller) and average pore diameters (d_p) were summarized in Table S2 in the ESM. The surface areas (S_{BET}) showed a decline as the Cu content increased, which probably due to the aggregation of Cu nanoparticles and blockage of the smaller pores [44]. The pore size distributions of the LOC/Cu-*x* catalysts were also significantly affected by the Cu content, especially when the Cu content was high (Fig. S5 in the ESM). The sharp decrease of S_{BET} and transformation from mesopores to macropores were observed when the Cu content was too high, indicating the serious aggregation of Cu. This agreed with the SEM images in Fig. 2. Such structure transformation would remarkably affect the catalytic activity and mass transfer during the reaction. Cu^{2+} is a paramagnetic ion possessing an unpaired electron, enabling the observation of Cu sites by electron paramagnetic spectroscopy (EPR) [45]. As clearly shown in

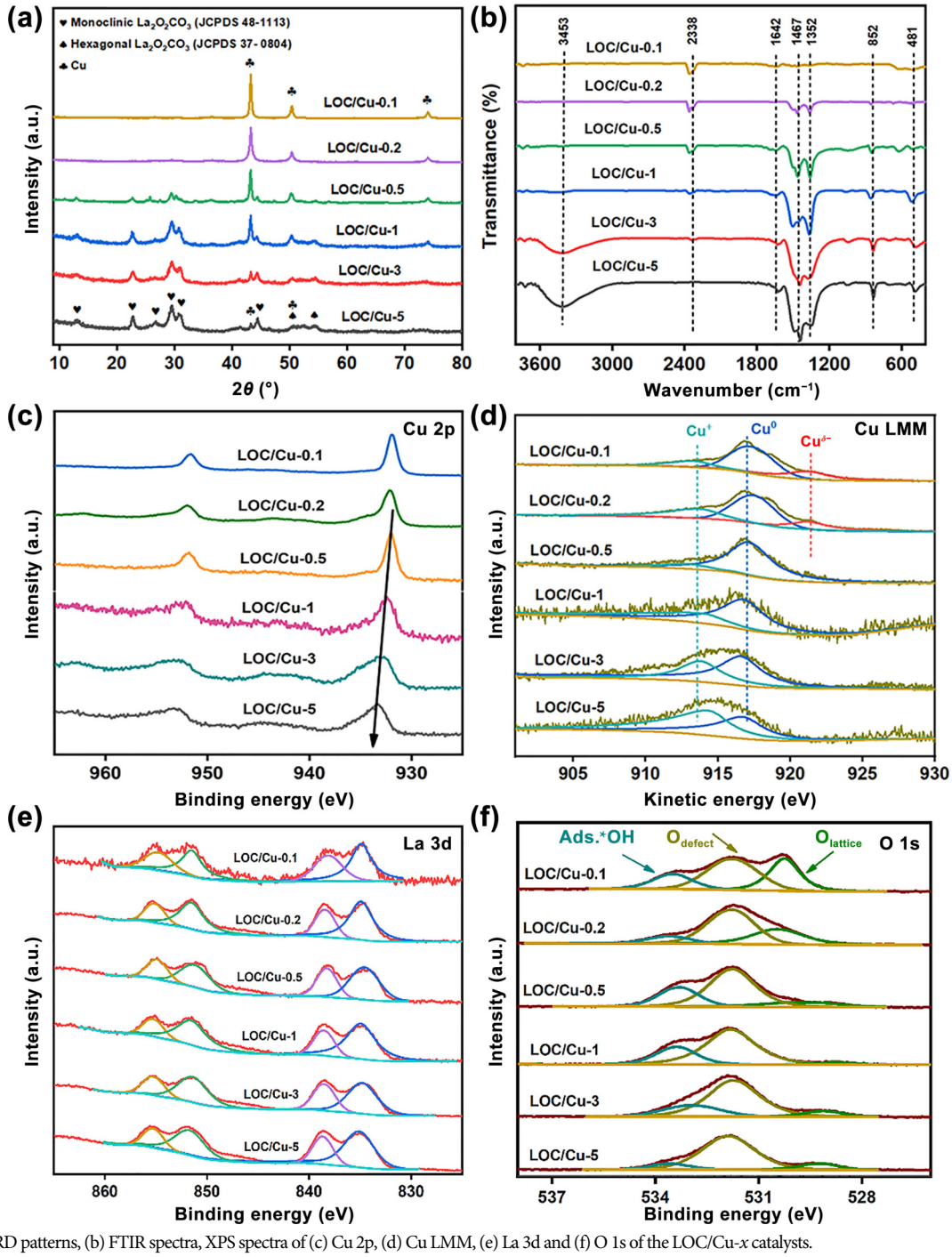

Figure 1 (a) XRD patterns, (b) FTIR spectra, XPS spectra of (c) Cu 2p, (d) Cu LMM, (e) La 3d and (f) O 1s of the LOC/Cu-*x* catalysts.

Fig. 3(b), the EPR signal intensity increased with decreasing Cu loading. This suggested the Cu dispersed better in the LOC/Cu-*x* catalysts at lower Cu contents, which engendered more surface Cu(II) species. However, all the samples exhibited similar spectral line shapes as a result of comparable properties and local electronic environment of Cu(II) species [46].

3.2 Catalytic reaction

The catalyst was appraised in the liquid solid phase reaction of CO_2 and H_2, where the solvent played an important role. Table 1 displayed the results of CO_2 hydrogenation using different solvents. Without a solvent, no product was detected and the reaction could hardly occur (entry 1). We tested some nonpolar solvents such as cyclohexane and n-decane, which showed poor reaction rates and low methanol selectivity (entries 2 and 3). When the polar solvents N-methyl-2-pyrrolidone (NMP) and H_2O were adopted, obviously higher catalytic activity and methanol selectivity were obtained (entries 4 and 5). Notably, the utilization of 1,3-dimethyl-2-imidazolidinone (DMI) solvent demonstrated the best reaction results, namely, the highest methanol selectivity and reaction activity (entry 6). Our previous study also demonstrated that some polar solvents were beneficial in the synthesis of alcohols [11]. Thus, we chose DMI as the reaction solvent in the following experiments.

In this work, the products of CO_2 hydrogenation contained

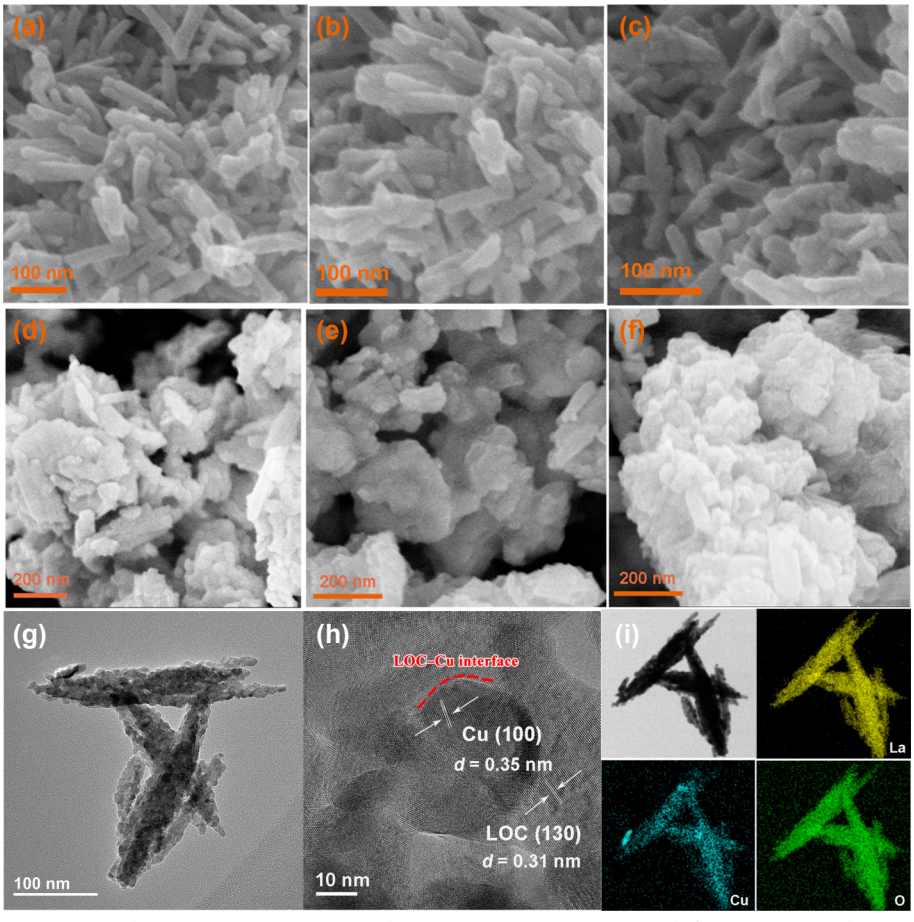

Figure 2 SEM images of (a) LOC/Cu-5, (b) LOC/Cu-3, (c) LOC/Cu-1, (d) LOC/Cu-0.5, (e) LOC/Cu-0.2 and (f) LOC/Cu-0.1 catalysts; (g) TEM image, (h) HRTEM image and (i) the EDS elemental mapping of the LOC/Cu-1 catalyst.

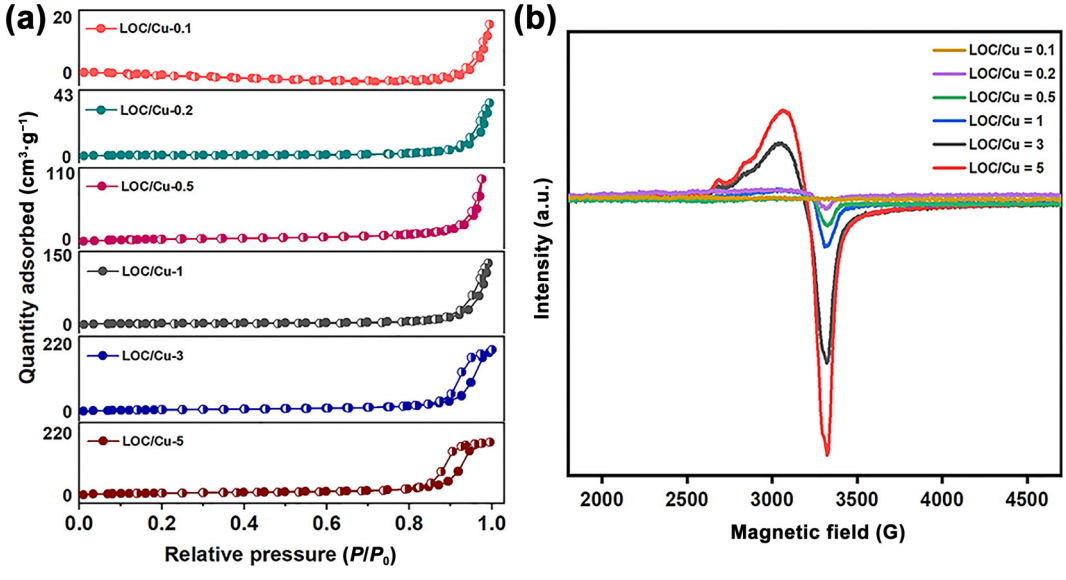

Figure 3 (a) N_2 adsorption–desorption isotherms and (b) EPR spectra of the LOC/Cu-*x* catalysts.

methanol, carbon monoxide and methane, tuning the selectivity of these products was a fascinating aspect of CO_2 hydrogenation. The Cu species were the active components of the LOC/Cu-*x* catalysts, because the pure LOC could not promote the reaction at all (Fig. 4(a)). The predominant product was methane when the catalysts of low Cu contents such as LOC/Cu-5 and LOC/Cu-3 were adopted. The major product turned to methanol with the increasing Cu content in the catalysts. The change of the major product might be attributed to the electron transfer between LOC and Cu at different Cu contents. At low Cu content, the electrons tended to transfer from Cu to LOC, and the positive Cu surface might help to accelerate the formation of methane. When the Cu content in

Table 1 CO_2 hydrogenation over the LOC/Cu-1 catalyst in different solvents[a]

Entries	Solvent	T (°C)	Selectivity (C-mol.%)			Activity ($mmol \cdot g_{Cu}^{-1} \cdot h^{-1}$)
			MeOH	CO	CH_4	
Entry 1	None	200	—	—	—	—
Entry 2	Cyclohexane	200	2.1	83.4	14.5	0.11
Entry 3	n-Decane	200	18.7	72.2	9.1	0.58
Entry 4	H_2O	200	63.2	30	6.8	8.9
Entry 5	NMP	200	14.3	27.5	58.2	4.9
Entry 6	DMI	200	85.5	9.1	5.4	13.3

[a]Reaction conditions: catalyst 20 mg, solvent 2 mL, initial pressure 8.0 MPa (H_2/CO_2 = 3:1), 200 °C, and 8 h.

catalyst became higher, the electron transfer from Cu to LOC dropped and the inverse electron transfer (from LOC to Cu) occurred, which might help to catalyze the generation of methanol via CO_2 hydrogenation. Among all the LOC/Cu-x catalysts, LOC/Cu-1 showed the highest methanol selectivity of 85.5% and the largest reaction rate of 13.3 $mmol \cdot g_{Cu}^{-1} \cdot h^{-1}$. The GC-MS spectra showed that methanol was the only liquid product of the reaction (Fig. S6 in the ESM).

Figure 4(b) illustrated the impact of temperature on the reaction. The catalytic activity and methanol selectivity were enhanced with the elevating temperature. The growth of methanol selectivity stopped and the elevation of reaction rate became unobvious when the temperature was higher than 200 °C. It seemed that higher temperature favored the RWGS reaction to produce CO, which restricted the further increase of the methanol selectivity. Therefore, 200 °C was the proper reaction temperature. At this temperature, the effect of H_2/CO_2 pressure ratios on the reaction was studied (Fig. 4(c)). As the H_2 pressure increased, the catalytic activity and methanol selectivity increased rapidly, and they became less distinct when the H_2/CO_2 ratio exceeded 3. Therefore, the H_2/CO_2 pressure ratio of 3 was fit for the reaction.

Finally, we investigated the recycling stability of the LOC/Cu-1 catalyst, the results were shown in Fig. 4(d). The selectivity of methanol maintained at about 85%, and the activity did not decline obviously after three runs, which suggested the good stability of the catalyst. The results of some recently reported Cu based catalysts for methanol synthesis via CO_2 hydrogenation were listed in Table S3 in the ESM, which demonstrated that the LOC/Cu-1 was an eminent catalyst for this reaction.

3.3 Mechanism discussion

As we had discussed above, the relative content of the Cu and LOC could remarkably affect their interaction, which engendered very different morphologies, porosities, crystal forms and surface valence. The chemisorption of the reactants (CO_2, H_2) on the catalyst surface was the initial and essential step for CO_2 hydrogenation [47]. We conducted the CO_2-temperature programmed desorption (TPD) analysis to measure the CO_2

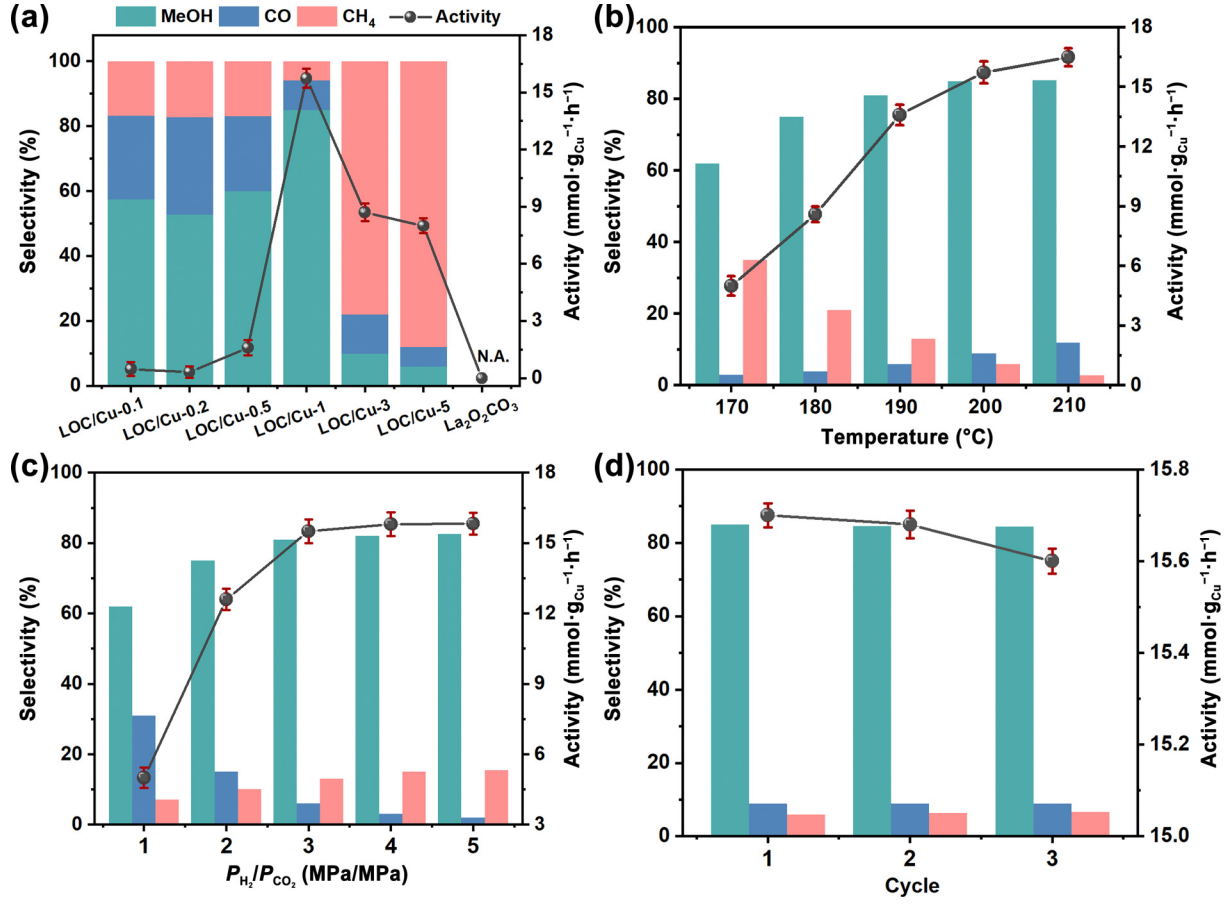

Figure 4 (a) Product selectivity and reaction activity of the LOC/Cu-x catalysts during CO_2 hydrogenation at 200 °C; effect of reaction temperature (b) and the pressure ratios of H_2 to CO_2 (c) on the CO_2 hydrogenation using the LOC/Cu-1 catalyst; (d) the results of the recycling experiments with the LOC/Cu-1 catalyst. Other conditions were the same as those in entry 6 of Table 1.

adsorption capacity of the LOC/Cu-*x* (Fig. 5(a)). The desorption peaks below 200 °C and between 200–400 °C were attributed to the desorption of CO_2 that were adsorbed onto the weak and moderate basic sites of the LOC/Cu-*x*, respectively [48]. Between 600–800 °C, the conversion of LOC ($La_2O_2CO_3$) to La_2O_3 led to the desorption of CO_2, so this desorption peak could not represent the quantity of strong basic sites [25]. In addition, the desorption peak in this region shifted to lower temperature with the introduction of Cu, indicating a strong interaction between Cu and LOC. As a whole, the capacity of CO_2 adsorption dropped with the increasing Cu content. However, the target reaction did not occur without Cu, which suggested that the crucial role of Cu in catalysing the reaction. The H_2 adsorption capacity of the catalysts near the reaction temperature was also important for the reaction, and the results of the H_2-TPD analysis were shown in Fig. 5(b). The results suggested that the capacity of H_2 adsorption within 150–300 °C was the smallest when Cu was the predominant component of the LOC/Cu-0.1. The LOC support might help to enhance the H_2 adsorption, and the adsorption capacity of H_2 over LOC/Cu-1 was the highest among the LOC/Cu-*x* catalysts.

By combining Figs. 4(a) and 5, we could deduce that the Cu component was the catalytic species but with very low adsorption capacity of CO_2 and H_2. The LOC itself had no catalytic capability but it might promote the adsorption of the reactant gases on the catalyst surface. The strong Cu–LOC interactions caused the transfer of electrons between Cu to LOC, which changed the chemical nature of the catalyst. There was also a synergy between Cu and LOC in adsorbing the reactant gases, because the capacity of H_2 adsorption on the LOC/Cu-1 catalyst could be much higher than that on the LOC. This could be one of the intrinsic causes of the eminent performance of the LOC/Cu-1 catalyst. The interaction of Cu and LOC might not only significantly accelerate the reaction rate but also evidently improve the methanol selectivity. We conducted the semi *in situ* XPS characterization of the LOC/Cu-1 catalyst after treatment with 3 MPa H_2 at 200 °C for 2 h (Fig. 6). The results demonstrated that minor Cu^+ still coexisted with Cu^0 on

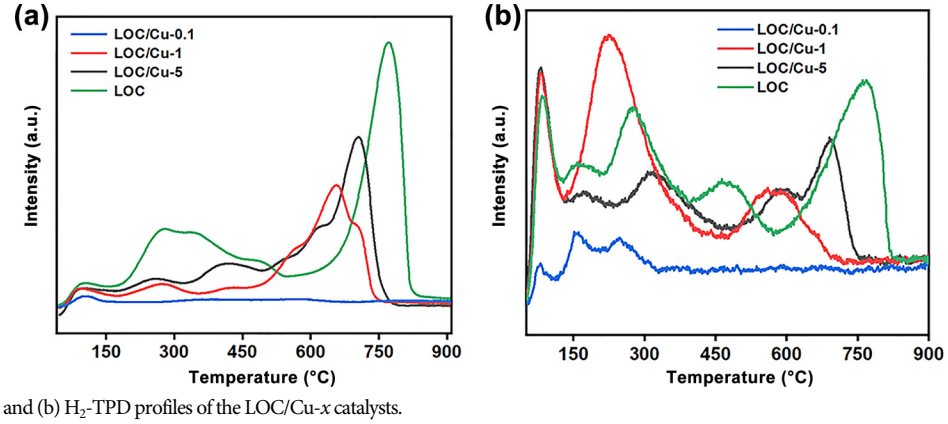

Figure 5 (a) CO_2-TPD and (b) H_2-TPD profiles of the LOC/Cu-*x* catalysts.

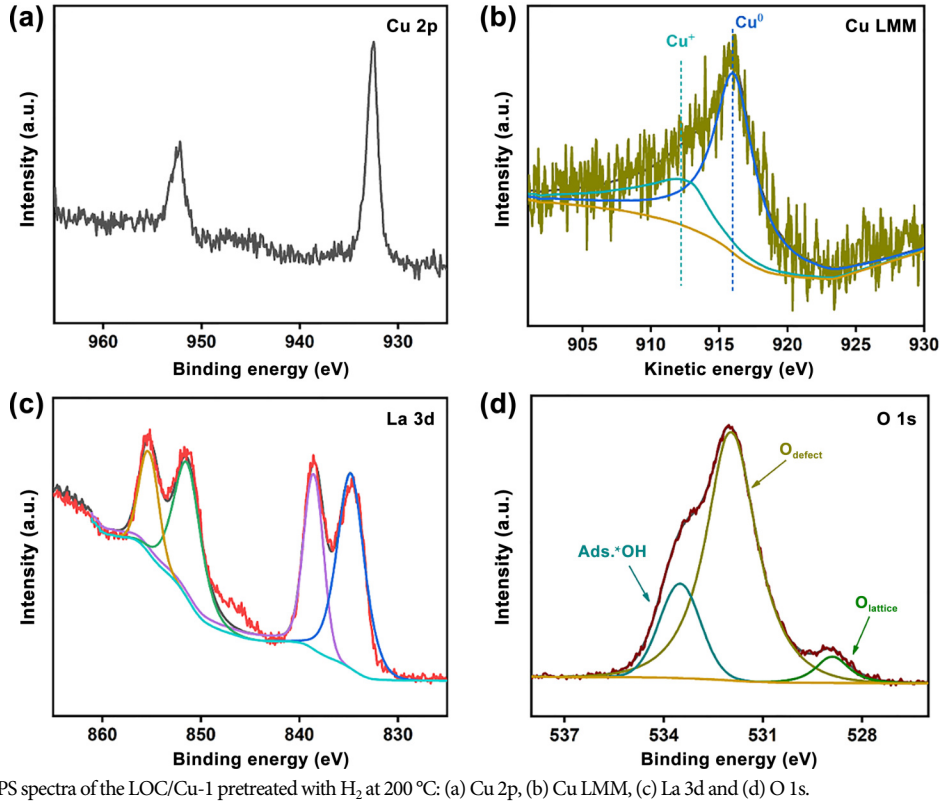

Figure 6 Semi *in situ* XPS spectra of the LOC/Cu-1 pretreated with H_2 at 200 °C: (a) Cu 2p, (b) Cu LMM, (c) La 3d and (d) O 1s.

the activated catalyst surface, which was similar to the prepared LOC/Cu-1 catalyst (Figs. 1(c)–1(f)). We further carried out the semi *in situ* study of the catalyst during the reaction of CO_2 with the chemisorbed H atoms at different temperatures, and no obvious valence alteration (Cu and La) were observed on the catalyst surface (Figs. 7(a)–7(c)). Finally, we tested the LOC/Cu-1 after the reaction by XPS measurement, as shown in Fig. 7(d). Compared with the catalyst before the reaction, the C 1s spectrum of the catalyst after the reaction hardly changed, which indicated that the C atoms in LOC/Cu-1 did not participate in the reaction, and the catalyst also showed excellent structural stability.

The reaction mechanisms on different kinds of catalysts have been well studied. There are two major reaction pathways reported for CO_2 hydrogenation to methanol: the formate (HCOO*) pathway and the CO* pathway [49]. Evident CO was detected after the LOC/Cu-1 catalyzed methanol synthesis via CO_2 hydrogenation (Fig. S7 in the ESM), which suggested the reaction might be through the CO* route. This speculation was supported by the reaction of 0.5 MPa CO and 1.5 MPa H_2, where remarkable methanol was observed (Fig. S8 in the ESM). In order to further verify our speculation, semi *in situ* XPS experiments were conducted to detect the intermediates formed at different adsorption temperatures on the LOC/Cu-1 pretreated with H_2 at reaction temperature (Fig. 8). The peak of binding energy at 292.2 eV corresponded to CO_2 adsorbed on the catalyst surface, while the peak of binding energy at 288.8 eV corresponded to carboxyl (O–C=O) groups. When the temperature rose from 50 to 200 °C, CO_2 adsorbed on the surface of LOC/Cu-1 catalyst was gradually transformed to carboxyl (O–C=O) group, which might further decompose into CO* [50]. The $^{13}CO_2$ labeling test confirmed that methanol was produced from reactant CO_2 rather than the CO_2 from LOC dissociation (Fig. S9 in the ESM).

The *in situ* FTIR were carried out to investigate the reaction process. Figure 9 showed the spectra of *in situ* FTIR for the LOC/Cu-1 catalyst exposed to flowing CO_2 at 150 °C, which was pre-treated with 10% H_2/Ar at 200 °C for 2 h. Several reaction intermediates were observed after the adsorption of CO_2 on the catalyst surface with active H atoms. The peaks at 2075 cm^{-1} were attributed to the stretching vibration of carbonyl groups bonded to Cu metal surfaces (Cu–C=O) [51], while the peaks at 1677 cm^{-1} corresponded to the carbonyl (C=O) stretching on hollow sites on Cu (100) [52]. The bands observed at 1580 cm^{-1} were associated with the O–C=O asymmetric stretching vibration [53], in agreement with the semi *in situ* XPS results (Fig. 8). The O–C=O could be further hydrogenated to produce C=O. Based on all the discussion above, we deduced that the CO_2 hydrogenation to methanol catalyzed by LOC/Cu-1 was through the CO* pathway.

4 Conclusions

In summary, a series of LOC/Cu-*x* nanorod catalysts were prepared via combining coprecipitation and calcination processes. The activity and selectivity of CO_2 hydrogenation to methanol were closely dependent on the composition of the LOC/Cu-*x* catalysts. The LOC had no catalytic capability and Cu was the major catalyst.

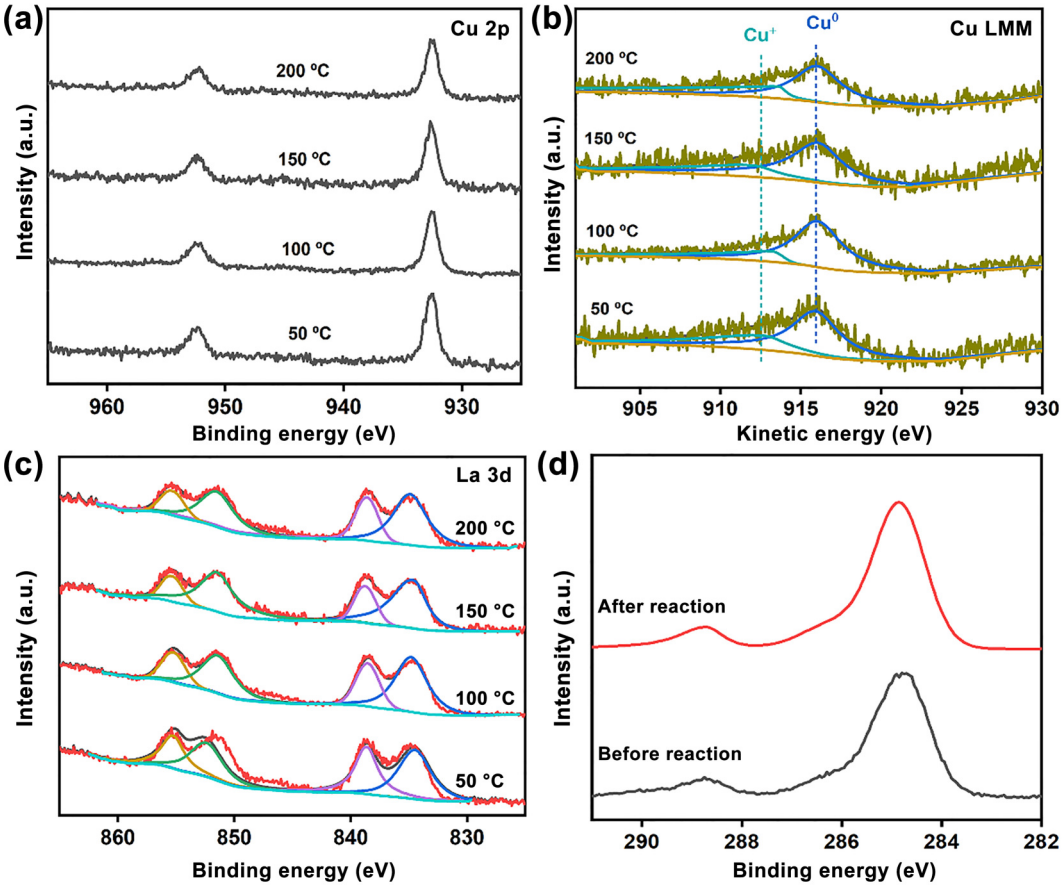

Figure 7 Semi *in situ* XPS spectra of the LOC/Cu-1 after CO_2 adsorption at different temperatures on the catalyst pretreated with H_2 at 200 °C: (a) Cu 2p, (b) Cu LMM and (c) La 3d. (d) XPS spectra (C 1s) of the LOC/Cu-1 catalyst before and after the CO_2 hydrogenation at optimal condition.

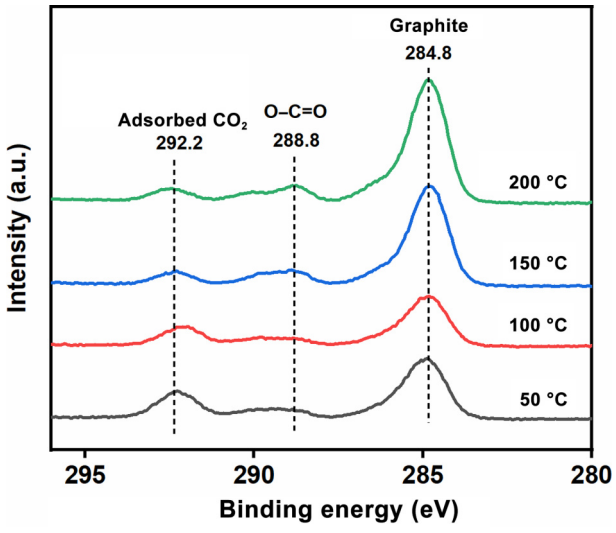

Figure 8 Semi *in situ* XPS spectra (C 1s) of the LOC/Cu-1 after CO_2 adsorption at different temperatures on the catalyst pretreated with H_2 at 200 °C.

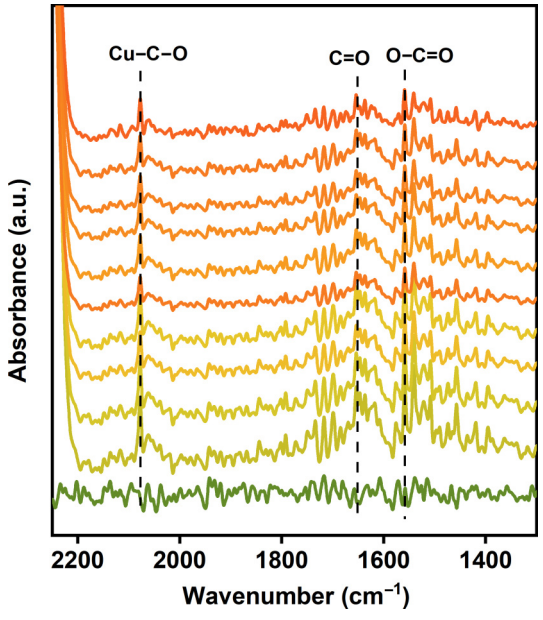

Figure 9 *In situ* FTIR spectra of the LOC/Cu-1 catalyst in flowing CO_2 after pretreatment with H_2 at 200 °C.

Methane was the predominant product when the LOC/Cu-5 catalyst was used. With the increase of the Cu content, the major product shifted from methane to methanol, demonstrating the crucial role of Cu in producing methanol. The best performance of methanol synthesis was obtained when LOC/Cu-1 was used as catalyst at 200 °C, with the reaction rate of 13.3 $mmol \cdot g_{Cu}^{-1} \cdot h^{-1}$ and methanol selectivity of 85.5%. Strong Cu–LOC interactions were observed by systematic characterizations of the catalysts. Besides the crystal structure, morphology and pore size distribution, the Cu–LOC interactions also influenced the mutual electron transfer between Cu and LOC, generating positive or negative charge on Cu surface. The Cu–LOC interactions also affected affinity of the catalyst toward CO_2 and H_2, which was crucial for the subsequent catalytic reaction. The mechanistic study suggested that the synthesis of methanol via CO_2 hydrogenation on the LOC/Cu-1 was through the CO* pathway. We believe that the effective catalysts designed in this work has promising potential of application, and the idea to prepare the catalysts is useful for design other effcient catalysts for CO_2 conversion.

Electronic Supplementary Material: Supplementary material (additional experimental details, XRD and XPS spectra, as well as TEM images and GC results) is available in the online version of this article at https://doi.org/10.26599/NR.2025.94907130.

Data availability

All data needed to support the conclusions in the paper are presented in the manuscript and the Electronic Supplementary Material. Additional data related to this paper may be requested from the corresponding author upon request.

Acknowledgements

The work was financially supported by the National Key Research and Development Program of China (No. 2024YFE0206500) and the National Science Foundation of China (Nos. 22033009, 22072156, 22073104 and 22121002).

Declaration of competing interest

All the contributing authors report no conflict of interests in this work.

Author contribution statement

J. H.: Writing manuscript and experimental design. B. Z., C. L. Y., Y. R. Z., L. B. Z., Y. Y. W., Y. W., Y. H. W., J. G., Y. L., and T. B. W.: Methodology and formal analysis. Z. J. Z. and B. G.: Resources and software. Q. L. Q.: Data curation, funding acquisition and supervision. H. X. W.: Data curation, project administration and validation. B. X. H.: Conceptualization, validation and funding acquisition. All the authors have approved the final manuscript.

Use of AI statement

None.

References

[1] He, M. Y.; Sun, Y. H.; Han, B. X. Green carbon science: Efficient carbon resource processing, utilization, and recycling towards carbon neutrality. *Angew. Chem.* **2022**, *134*, e202112835.

[2] He, M. Y.; Sun, Y. H.; Han, B. X. Green carbon science: Scientific basis for integrating carbon resource processing, utilization, and recycling. *Angew. Chem., Int. Ed.* **2013**, *52*, 9620–9633.

[3] Zhang, S. N.; Wu, Z. X.; Liu, X. F.; Hua, K. M.; Shao, Z. L.; Wei, B. Y.; Huang, C. J.; Wang, H.; Sun, Y. H. A short review of recent advances in direct CO_2 hydrogenation to alcohols. *Top. Catal.* **2021**, *64*, 371–394.

[4] Wu, Y. F.; Lu, X. T.; Cui, P. F.; Jia, W. Y.; Zhou, J.; Wang, Y.; Zahid, H.; Wu, Y. X.; Umer Rafique, M.; Yin, X. et al. Enhancing alkyne semi-hydrogenation through engineering metal-support interactions of Pd on oxides. *Nano Res.* **2024**, *17*, 3707–3713.

[5] Guo, Z. R.; Zhang, X.; Li, X. Y.; Cui, C.; Zhang, Z. L.; Li, H. S.; Zhang, D. X.; Li, J. Y.; Xu, X. Y.; Zhang, J. T. Enhanced charge separation by incomplete calcination modified Co-doped TiO_2 nanoparticle for isothiazolinone photocatalytic degradation. *Nano Res.* **2024**, *17*, 4834–4843.

[6] Li, H. J.; Fang, W.; Wang, L. X.; Liu, Y. F.; Liu, L. J.; Sun, T. L.; Liao, C. Q.; Zhu, Y. H.; Wang, L.; Xiao, F. S. Physical regulation of

copper catalyst with a hydrophobic promoter for enhancing CO_2 hydrogenation to methanol. *Innovation* **2023**, *4*, 100445.
[7] Asare Bediako, B. B.; Qian, Q. L.; Han, B. X. Synthesis of C_{2+} chemicals from CO_2 and H_2 via C–C bond formation. *Acc. Chem. Res.* **2021**, *54*, 2467–2476.
[8] Qian, Q. L.; Han, B. X. Transformation of CO_2 and H_2 to C_{2+} chemicals and fuels. *Natl. Sci. Rev.* **2023**, *10*, nwad160.
[9] Cui, M.; Qian, Q. L.; Zhang, J. J.; Wang, Y.; Asare Bediako, B. B.; Liu, H. Z.; Han, B. X. Liquid fuel synthesis via CO_2 hydrogenation by coupling homogeneous and heterogeneous catalysis. *Chem* **2021**, *7*, 726–737.
[10] Qian, Q. L.; Zhang, J. J.; Cui, M.; Han, B. X. Synthesis of acetic acid via methanol Hydrocarboxylation with CO_2 and H_2. *Nat. Commun.* **2016**, *7*, 11481.
[11] He, Z. H.; Qian, Q. L.; Ma, J.; Meng, Q. L.; Zhou, H. C.; Song, J. L.; Liu, Z. M.; Han, B. X. Water-enhanced synthesis of higher alcohols from CO_2 hydrogenation over a Pt/Co_3O_4 catalyst under milder conditions. *Angew. Chem., Int. Ed.* **2016**, *55*, 737–741.
[12] He, Z. H.; Cui, M.; Qian, Q. L.; Zhang, J. J.; Liu, H. Z.; Han, B. X. Synthesis of liquid fuel via direct hydrogenation of CO_2. *Proc. Natl. Acad. Sci. USA* **2019**, *116*, 12654–12659.
[13] He, J.; Wang, H. X.; Wang, Y.; Zhang, Y. R.; Li, Y.; Zhang, L. B.; Wang, Y. Y.; Yu, C. L.; Jia, S. H.; Qian, Q. L. et al. Synthesis of $InZrO_x$ nanosheets and its application in CO_2 hydrogenation to methanol. *Appl. Surf. Sci.* **2024**, *664*, 160198.
[14] Jiang, F.; Yang, Y.; Wang, L.; Li, Y. F.; Fang, Z. H.; Xu, Y. B.; Liu, B.; Liu, X. H. Dependence of copper particle size and interface on methanol and CO formation in CO_2 hydrogenation over Cu@ZnO catalysts. *Catal. Sci. Technol.* **2022**, *12*, 551–564.
[15] Grabow, L. C.; Mavrikakis, M. Mechanism of methanol synthesis on Cu through CO_2 and CO hydrogenation. *ACS Catal.* **2011**, *1*, 365–384.
[16] Figueiredo, R. T.; Martínez-Arias, A.; Granados, M. L.; Fierro, J. L. G. Spectroscopic evidence of Cu–Al interactions in Cu–Zn–Al mixed oxide catalysts used in CO hydrogenation. *J. Catal.* **1998**, *178*, 146–152.
[17] Cui, X. J.; Chen, S.; Yang, H. H.; Liu, Y. Q.; Wang, H. F.; Zhang, H.; Xue, Y. F.; Wang, G. F.; Niu, Y. L.; Deng, T. S. et al. Improving methanol selectivity in CO_2 hydrogenation by tuning the distance of Cu on catalyst. *Appl. Catal. B: Environ.* **2021**, *298*, 120590.
[18] Liao, F. L.; Huang, Y. Q.; Ge, J. W.; Zheng, W. R.; Tedsree, K.; Collier, P.; Hong, X. L.; Tsang, S. C. Morphology-dependent interactions of ZnO with Cu nanoparticles at the materials' interface in selective hydrogenation of CO_2 to CH_3OH. *Angew. Chem.* **2011**, *123*, 2210–2213.
[19] Bansode, A.; Tidona, B.; Von Rohr, P. R.; Urakawa, A. Impact of K and Ba promoters on CO_2 hydrogenation over Cu/Al_2O_3 catalysts at high pressure. *Catal. Sci. Technol.* **2013**, *3*, 767–778.
[20] Zhao, H. B.; Yu, R. F.; Ma, S. C.; Xu, K. Z.; Chen, Y.; Jiang, K.; Fang, Y.; Zhu, C. X.; Liu, X. C.; Tang, Y. et al. The role of Cu_1–O_3 species in single-atom Cu/ZrO_2 catalyst for CO_2 hydrogenation. *Nat. Catal.* **2022**, *5*, 818–831.
[21] Huang, C. L.; Wen, J. J.; Sun, Y. H.; Zhang, M. Y.; Bao, Y. F.; Zhang, Y. D.; Liang, L.; Fu, M. L.; Wu, J. L.; Ye, D. Q. et al. CO_2 Hydrogenation to methanol over Cu/ZnO plate model catalyst: Effects of reducing gas induced Cu nanoparticle morphology. *Chem. Eng. J.* **2019**, *374*, 221–230.
[22] Wu, C. Y.; Lin, L. L.; Liu, J. J.; Zhang, J. P.; Zhang, F.; Zhou, T.; Rui, N.; Yao, S. Y.; Deng, Y. C.; Yang, F. et al. Inverse ZrO_2/Cu as a highly efficient methanol synthesis catalyst from CO_2 hydrogenation. *Nat. Commun.* **2020**, *11*, 5767.
[23] Zhang, R.; Wang, X.; Wang, K.; Wang, H. L.; Liu, L.; Wu, X. T.; Geng, B. K.; Chu, X.; Song, S. Y.; Zhang, H. J. Synergism of ultrasmall Pt clusters and basic $La_2O_2CO_3$ supports boosts the reverse water gas reaction efficiency. *Adv. Energy Mater.* **2023**, *13*, 2203806.
[24] Wang, F.; Zhang, Z. N.; Wei, X. J.; Fang, Q. H.; Jiang, X. M. The shape effect of $La_2O_2CO_3$ in $Pd/La_2O_2CO_3$ catalyst for selective hydrogenation of cinnamaldehyde. *Appl. Catal. A: Gen.* **2017**, *543*, 196–200.
[25] Dai, Y. H.; Xu, M.; Wang, Q. J.; Huang, R.; Jin, Y. Y.; Bian, B.; Tumurbaatar, C.; Ishtsog, B.; Bold, T.; Yang, Y. H. Enhanced activity and stability of $Ni/La_2O_2CO_3$ catalyst for CO_2 methanation by metal–carbonate interaction. *Appl. Catal. B: Environ.* **2020**, *277*, 119271.
[26] Li, X. Y.; Li, D.; Tian, H.; Zeng, L.; Zhao, Z. J.; Gong, J. L. Dry reforming of methane over Ni/La_2O_3 nanorod catalysts with stabilized Ni nanoparticles. *Appl. Catal. B: Environ.* **2017**, *202*, 683–694.
[27] Lv, J. N.; Wang, D. C.; Wang, M. Y.; Li, Y.; Jin, L. J.; Hu, H. Q. Integrated coal pyrolysis with dry reforming of low carbon alkane over Ni/La_2O_3 to improve tar yield. *Fuel* **2020**, *266*, 117092.
[28] Xu, L. J.; Liu, W. M.; Zhang, X.; Tao, L. L.; Xia, L. H.; Xu, X. L.; Song, J. W.; Zhou, W. F.; Fang, X. Z.; Wang, X. Ni/La_2O_3 catalysts for dry reforming of methane: Insights into the factors improving the catalytic performance. *ChemCatChem* **2019**, *11*, 2887–2899.
[29] Muroyama, H.; Tsuda, Y.; Asakoshi, T.; Masitah, H.; Okanishi, T.; Matsui, T.; Eguchi, K. Carbon dioxide methanation over Ni catalysts supported on various metal oxides. *J. Catal.* **2016**, *343*, 178–184.
[30] Pakhare, D.; Schwartz, V.; Abdelsayed, V.; Haynes, D.; Shekhawat, D.; Poston, J.; Spivey, J. Kinetic and mechanistic study of dry (CO_2) reforming of methane over Rh-substituted $La_2Zr_2O_7$ pyrochlores. *J. Catal.* **2014**, *316*, 78–92.
[31] Irusta, S.; Cornaglia, L. M.; Lombardo, E. A. Effects of rhodium and platinum on the reactivity of lanthanum phases. *Mater. Chem. Phys.* **2004**, *86*, 440–447.
[32] Park, C. Y.; Nguyen-Phu, H.; Shin, E. W. Glycerol carbonation with CO_2 and $La_2O_2CO_3$/ZnO catalysts prepared by two different methods: Preferred reaction route depending on crystalline structure. *Mol. Catal.* **2017**, *435*, 99–109.
[33] Hussain, S. K.; Nagaraju, G.; Pavitra, E.; Raju, G. S. R.; Yu, J. S. $La(OH)_3$: Eu^{3+} and La_2O_3: Eu^{3+} nanorod bundles: Growth mechanism and luminescence properties. *CrystEngComm* **2015**, *17*, 9431–9442.
[34] Shieh, Y. T.; Liu, K. H. The effect of carbonyl group on sorption of CO_2 in glassy polymers. *J. Supercrit. Fluids* **2003**, *25*, 261–268.
[35] Mu, Q. Y.; Wang, Y. D. Synthesis, characterization, shape-preserved transformation, and optical properties of $La(OH)_3$, $La_2O_2CO_3$, and La_2O_3 nanorods. *J. Alloys Compd.* **2011**, *509*, 396–401.
[36] Tian, R.; Yang, S.; Han, Z. Y.; Sun, Y.; Wang, Y. X.; Wu, C.; Zhang, Q.; Liu, J. Y.; Lu, X. L.; Zhang, Z. W. Efficient removal of phosphate through adsorption by acidified diatomite loaded with $La_2O_2CO_3$. *New J. Chem.* **2023**, *47*, 15201–15208.
[37] Levan, T.; Che, M.; Tatibouet, J. M.; Kermarec, M. Infrared study of the formation and stability of $La_2O_2CO_3$ during the oxidative coupling of methane on La_2O_3. *J. Catal.* **1993**, *142*, 18–26.
[38] Dong, S. X.; Wang, Y. L.; Zhao, Y. W.; Zhou, X. H.; Zheng, H. L. La^{3+}/$La(OH)_3$ loaded magnetic cationic hydrogel composites for phosphate removal: Effect of lanthanum species and mechanistic study. *Water Res.* **2017**, *126*, 433–441.
[39] Zhu, Y.; Li, B. L.; Zhao, C. Cu nanoparticles supported on core–shell MgO-La_2O_3 catalyzed hydrogenolysis of furfuryl alcohol to pentanediol. *J. Catal.* **2022**, *410*, 42–53.
[40] Liang, Z. Q.; Zhuang, T. T.; Seifitokaldani, A.; Li, J.; Huang, C. W.; Tan, C. S.; Li, Y.; De Luna, P.; Dinh, C. T.; Hu, Y. et al. Copper-on-nitride enhances the stable electrosynthesis of multi-carbon products from CO_2. *Nat. Commun.* **2018**, *9*, 3828.
[41] Zhao, H. H.; Zhang, W. Z.; Song, H. L.; Zhao, J.; Yang, J.; Yan, L.; Qiao, B. T.; Chou, L. J. Highly coke-resistant Ni-$La_2O_2CO_3$ catalyst with low Ni loading for dry reforming of methane with carbon dioxide. *Catal. Today* **2022**, *402*, 189–201.
[42] Chen, G.; Han, B. Q.; Deng, S. J.; Wang, Y.; Wang, Y. D. Lanthanum dioxide carbonate $La_2O_2CO_3$ nanorods as a sensing material for chemoresistive CO_2 gas sensor. *Electrochim. Acta* **2014**, *127*, 355–361.

[43] Rui, N.; Wang, Z. Y.; Sun, K. H.; Ye, J. Y.; Ge, Q. F.; Liu, C. J. CO_2 hydrogenation to methanol over Pd/In_2O_3: Effects of Pd and oxygen vacancy. *Appl. Catal. B: Environ.* **2017**, *218*, 488–497.

[44] Hu, B.; Yin, Y. Z.; Zhong, Z. X.; Wu, D. D.; Liu, G. L.; Hong, X. L. Cu@ZIF-8 derived inverse ZnO/Cu catalyst with sub-5 nm ZnO for efficient CO_2 hydrogenation to methanol. *Catal. Sci. Technol.* **2019**, *9*, 2673–2681.

[45] Giordanino, F.; Vennestrøm, P. N. R.; Lundegaard, L. F.; Stappen, F. N.; Mossin, S.; Beato, P.; Bordiga, S.; Lamberti, C. Characterization of Cu-exchanged SSZ-13: A comparative FTIR, UV–Vis, and EPR study with Cu-ZSM-5 and Cu-β with similar Si/Al and Cu/Al ratios. *Dalton Trans.* **2013**, *42*, 12741–12761.

[46] Zhang, Y. N.; Peng, Y.; Li, J. H.; Groden, K.; McEwen, J. S.; Walter, E. D.; Chen, Y.; Wang, Y.; Gao, F. Probing active-site relocation in Cu/SSZ-13 SCR catalysts during hydrothermal aging by *in situ* EPR spectroscopy, kinetics studies, and DFT calculations. *ACS Catal.* **2020**, *10*, 9410–9419.

[47] Guo, X. M.; Mao, D. S.; Lu, G. Z.; Wang, S.; Wu, G. S. The influence of La doping on the catalytic behavior of Cu/ZrO_2 for methanol synthesis from CO_2 hydrogenation. *J. Mol. Catal. A: Chem.* **2011**, *345*, 60–68.

[48] Li, Y. J.; Liu, H. M.; Ma, L.; Liu, J. X.; He, D. H. Transforming glycerol and CO_2 into glycerol carbonate over $La_2O_2CO_3$-ZnO catalyst—A case study of the photo-thermal synergism. *Catal. Sci. Technol.* **2021**, *11*, 1007–1013.

[49] Zhong, J. W.; Yang, X. F.; Wu, Z. L.; Liang, B. L.; Huang, Y. Q.; Zhang, T. State of the art and perspectives in heterogeneous catalysis of CO_2 hydrogenation to methanol. *Chem. Soc. Rev.* **2020**, *49*, 1385–1413.

[50] Yang, C. S.; Pei, C. L.; Luo, R.; Liu, S. H.; Wang, Y. N.; Wang, Z. Y.; Zhao, Z. J.; Gong, J. L. Strong electronic oxide-support interaction over In_2O_3/ZrO_2 for highly selective CO_2 hydrogenation to methanol. *J. Am. Chem. Soc.* **2020**, *142*, 19523–19531.

[51] Liu, X. L.; Fu, G. Y.; Lang, Q. L.; Ding, R. Q.; Guo, Q. S.; Liang, K.; Gao, S. M.; Yang, X. B.; Yu, B. Reaction intermediates recognized by *in situ* FTIR spectroscopy in CO_2 hydrogenation over the Cu/ZnO/SPP-zeolite catalyst. *RSC Appl. Interfaces*, in press, DOI: 10.1039/D4LF00266K.

[52] Pérez-Gallent, E.; Figueiredo, M. C.; Calle-Vallejo, F.; Koper, M. T. M. Spectroscopic observation of a hydrogenated CO dimer intermediate during CO reduction on Cu (100) electrodes. *Angew. Chem., Int. Ed.* **2017**, *56*, 3621–3624.

[53] Deng, S. M.; Wang, R. H.; Feng, X. Z.; Zheng, R. J.; Gong, S. K.; Chen, X. H.; Shangguan, Y. Z.; Deng, L. L.; Tang, H.; Dai, H. et al. Dual Lewis acid-base sites regulate silver-copper bimetallic oxide nanowires for highly selective photoreduction of carbon dioxide to methane. *Angew. Chem.* **2023**, *135*, e202309625.